Separation and Purification Technology 174 (2017) 425–431

Contents lists available at ScienceDirect

Separation and Purification Technology

journal homepage: www.elsevier.com/locate/seppur

Spectroscopic and modeling investigation of efficient removal of U(VI) on a novel magnesium silicate/diatomite

Songhua Lu [a,b], Jiansheng Hu [a], Changlun Chen [a], Xiaojun Chen [c], Yu Gong [c], Yubing Sun [a,*], Xiaoli Tan [a,*]

[a] Institute of Plasma Physics, Chinese Academy of Sciences, P.O. Box 1126, Hefei 230031, PR China
[b] University of Science and Technology of China, Hefei 230026, PR China
[c] Institute of Nuclear Physics and Chemistry, China Academy of Engineering Physics, Mianyang 621900, PR China

ARTICLE INFO

Article history:
Received 1 August 2016
Received in revised form 2 September 2016
Accepted 2 September 2016
Available online 2 November 2016

Keywords:
Sorption
U(VI)
Silicate composites
Modeling

ABSTRACT

A novel magnesium silicate/diatomite sorbent (MSD) was fabricated using a facile hydrothermal method. The interaction mechanism of U(VI) on MSD was investigated by batch, spectroscopic and modeling techniques. The maximum adsorption capacity of MSD for U(VI) (31.54 mg/g) is significantly higher than that of diatomite (12.74 mg/g). XPS analysis indicated that the oxygen-containing groups (e.g., Si—OH) of MSD were responsible for the high efficient removal of U(VI) from aqueous solutions. The fitted results of surface complexation modeling showed that the adsorption of U(VI) on MSD at pH < 4.0 and pH > 4.5 was attributed to cation exchange and inner-sphere surface complexation, respectively. These findings suggested that MSD could be a favorable sorbent for the efficient removal of U(VI) in the environmental cleanup.

1. Introduction

Uranium as a kind of actinide has greatly been concerned due to its radioactivity, significant biological and chemical toxicity [1,2]. Therefore, the removal of uranium from contaminated water has attracted much attention by a variety of methods such as sorption [3,4], membrane separation [5], ion exchange [6]. Among these methods, the sorption process is an attractive treatment method due to its inexpensive, readily available, highly efficient, easy to use, environmentally friendly, and so on [7,8]. Owing to its high porosity and surface activity, diatomite has been extensively used to remove a variety of environmental pollutants in recent years [7,9,10]. However, the limited adsorption capacity of diatomite is rather difficult to apply in practice.

In order to improve the sorption performance, diatomite was usually modified through various treatment methods such as acid and alkali treatment [11,12], inorganic and organic modifier [13–17]. Among them, the inorganic substance deposited diatomite composite materials had the high sorption capacity for heavy metal ions. Du et al. found that the α-Fe_2O_3 and MnO_2 nanowires deposited diatomite were highly efficient adsorbents for the removal of arsenic or chromium ions [13–15]. Meanwhile, the magnesium silicate composites were also recently synthesized to remove organic pollutants and heavy metals [18–22]. Zhang et al. [22] report that the hierarchical iron oxide@magnesium silicate magnetic nanorods exhibited strong sorption ability with methylene blue. Wang et al. [21] found that the magnesium silicate hollow spheres have the high sorption capacity for methylene blue. Ou et al. [19] discovered that Fe_3O_4@$MgSiO_3$ sub-microspheres were a promising sorbent for Pb^{2+} ions removal from aqueous solution. However, most of these syntheses involve tedious procedures and the longer react time, which greatly reduced the efficiency for the synthesis process. However, magnesium silicate/diatomite (MSD) composite can be easily synthesized through a facile, rapid and green hydrothermal method. This method highly enhanced the syntheses efficiency, which was due to its omitted the inorganic substance growth process or the SiO_2 spheres synthesis process. To the authors' knowledge, the investigation of U(VI) sorption on magnesium silicate/diatomite (MSD) composite has been rarely reported.

The objectives of this study were (1) to characterize morphology and surface groups of MSD by using scanning electron microscopy (SEM), Fourier transform infrared spectroscopy (FT-IR), X-ray diffraction (XRD) and X-ray photoelectron spectroscopy (XPS); (2) to investigate the effect of water chemistry on the high efficient removal of U(VI) on MSD by batch techniques; (3) to determine the sorption mechanisms between MSD and U(VI) by X-ray photoelectron spectroscopy (XPS) and surface complexation modeling. The highlight of this study is MSD as a promising adsor-

* Corresponding authors.
E-mail addresses: sunyb@ipp.ac.cn (Y. Sun), tanxl@ipp.ac.cn (X. Tan).

http://dx.doi.org/10.1016/j.seppur.2016.09.052
1383-5866/

bent for the preconcentration and immobilization of uranium in environmental pollution management.

2. Experimental

2.1. Materials and methods

All chemicals in analytical purity were purchased from Shanghai Chemical Reagent Co. Ltd (China) and were used without further purification. U(VI) stock solution (120 mg/L) was obtained by dissolving uranyl nitrate ($UO_2(NO_3)_2{\cdot}6H_2O$, analytical reagent) into deionized water. And the main component of the diatomite sample was SiO_2 ($\geqslant$85.0%).

The MSD was synthesized by the modified hydrothermal method [21]. Briefly, 0.1 g diatomite was homogeneously dispersed in 15 mL deionized water, while 0.01 mol ammonia chloride, 0.003 mol magnesium chloride and 4.8 mL of 28% ammonia solution were dissolved in 20 mL deionized water. Two solutions were mixed under vigorous stirring conditions and then were transferred into a Teflon-lined stainless-steel autoclave (100 mL) and sealed to heat at 160 °C for 2 h. The MSD was obtained by washing it with deionized water and ethanol sequent and then freeze-dried overnight.

2.2. Characterization

The morphologies of raw diatomite and MSD were illustrated by scanning electron microscopy (SEM). The surface groups of raw diatomite and MSD were characterized using Fourier transform infrared spectroscopy (FT-IR) (Perkin Elmer spectrum 100, America) in pressed KBr pellets. The spectral resolution was set to 1 cm^{-1}, and 150 scans were collected for each spectrum. The identification of the diatomite and MSD were recorded by Rigaku X-ray diffractometer (MAC Science Co. M18XHF diffractometer) with Cu Kα radiation (λ = 0.1541 nm). The specific surface areas were measured by Brunauer-Emmett-Teller (BET) method. The nitrogen isotherms at 77 K were measured using sorption instrument (TriStarII, Micromeritics Company, USA) to evaluate their pore structures. The zeta potentials of diatomite and MSD were measured by ZETASIZER, Nano-ZS90. The change in surface groups for MSD before and after U(VI) sorption were characterized the X-ray photoelectron spectroscopy (XPS) on an ESCALab 220I-XL system (Thermo-VG Scientific). The XPS data were processed using the XPSPEAK software (version 4.1).

2.3. Sorption experiments

The sorption experiments were conducted in 10 mL polyethylene test tubes by using batch technique. The raw diatomite or MSD and $NaNO_3$ solution were added to pre-equilibrate 24 h and then U(VI) solution was added into the suspensions. The pH of suspensions was adjusted to the desired values by adding negligible amount of 0.01–1.0 mol/L HNO_3 or NaOH solutions. After the suspensions were shaken for 24 h, the liquid and solid phases were separated by centrifugation it at 9000 rpm for 20 min.

The concentration of U(VI) in supernatant was determined using Fluorolog-3 fluorescence spectrometer (Johin-Yvon-SPEX instruments, New Jersey). The amount of U(VI) sorbed on diatomite or MSD was calculated from the difference between the initial concentration (C_0) and the equilibrium concentration (C_e). The sorption percentage (sorption %) and the amount (q_e) of U(VI) sorbed on diatomite or MSD after equilibrium were expressed from the following Eqs. (1) and (2):

$$Sorption\ \% = \frac{C_0 - C_e}{C_0} \times 100\% \quad (1)$$

$$q_e = \frac{(C_0 - C_e) \times V}{m} \quad (2)$$

where C_0 and C_e (mg/L) are the initial and the equilibrium concentration of U(VI) remained in solution, respectively. m (g) is the mass of diatomite or MSD, and V (L) is the volume of suspension. All the experimental data were the average of triplicate experiments and the relative errors of data were less than ±5%.

2.4. Surface complexation modeling

The pH-dependent adsorption of U(VI) on MSD were simulated by using the surface complexation modeling employing diffuse layer model with the aid of Visual MINTEQ codes [23]. Diffuse layer model assumed that amphoteric hydroxide functional groups (SOH) can be reacted with U(VI) species from aqueous solutions. The protonation and deprotonation constants ($\log K^+$, $\log K^-$) are given the following Eqs. (3) and (4):

$$SOH + H^+ = SOH_2^+ \quad \log K^+ = \log\left(\left[SOH_2^+\right]/([SOH][H^+])\right) \quad (3)$$

$$SOH = SO^- + H^+ \quad \log K^- = \log([SO^-][H^+]/[SOH]) \quad (4)$$

Two surface complexation reactions were selected in conjunction with batch adsorption data, which can be described as Eqs. (5) and (6):

$$2XNa + UO_2^{2+} = 2Na^+ + X_2UO_2 \quad \log K_1 = \log([X_2UO_2][Na^+]^2/([XNa]^2\left[UO_2^{2+}\right]) \quad (5)$$

$$SOH + UO_2^{2+} = SOUO_2^+ + H^+ \quad \log K_2 = \log(\left[SOUO_2^+\right][H^+]/([SOH]UO_2^{2+}]) \quad (6)$$

At adjustable parameters, the site density (Ns, sites/m^2) can be calculated by Eq. (7):

$$N_s = Nt \times N_A/(C_s \times S_A) \quad (7)$$

where Cs (g/L) refer to solid concentration, respectively. N_A (sites/-mol) and S_A (m^2/g) are Avogadro constants and specific surface area, respectively. The total reactive sites concentration (Nt, mol/L) can be obtained by fitting the potentiometric data. Hence, the site density for sepiolite was calculated to be 4.48 sites/nm^2 for U(VI), which range from 2 to 20 sites/nm^2 for oxides [24].

3. Results and discussion

3.1. Characterization

Fig. 1 shows the characterization of raw diatomite and MSD sample. As shown by SEM in Fig. 1A, the diatomite sample possessed a disc-like morphology with a uniform ordered porous structure. For MSD, a large number of nanowires remained porous structure was clearly observed (Fig. 1B). As shown in Fig. 1C, the FT-IR spectrum of raw diatomite showed major adsorption bands at 3445 and 1630 cm^{-1} were attributed to the stretching and bending vibration of water molecules, respectively [25,26]. The bands at 1097, 793 and 481 cm^{-1} were responded to the asymmetric stretching, symmetric stretching and bending vibration of Si—O—Si, respectively [27,28]. The broad band at 3445 cm^{-1} was due to the stretching vibration of Si—O—H on the surface [29]. For MSD, some typical absorption bands (from 1097 to 1095 cm^{-1}, from 481 to 476 cm^{-1}) were shifted to the lower wavenumbers, which could be ascribed to the changes in the microenvironment of these groups. As shown in Fig. 1D, the XRD patterns of diatomite showed the typical crystalline diffraction peaks at 2θ = 22.0, 28.4, 31.5 and 36.1°, which matched the

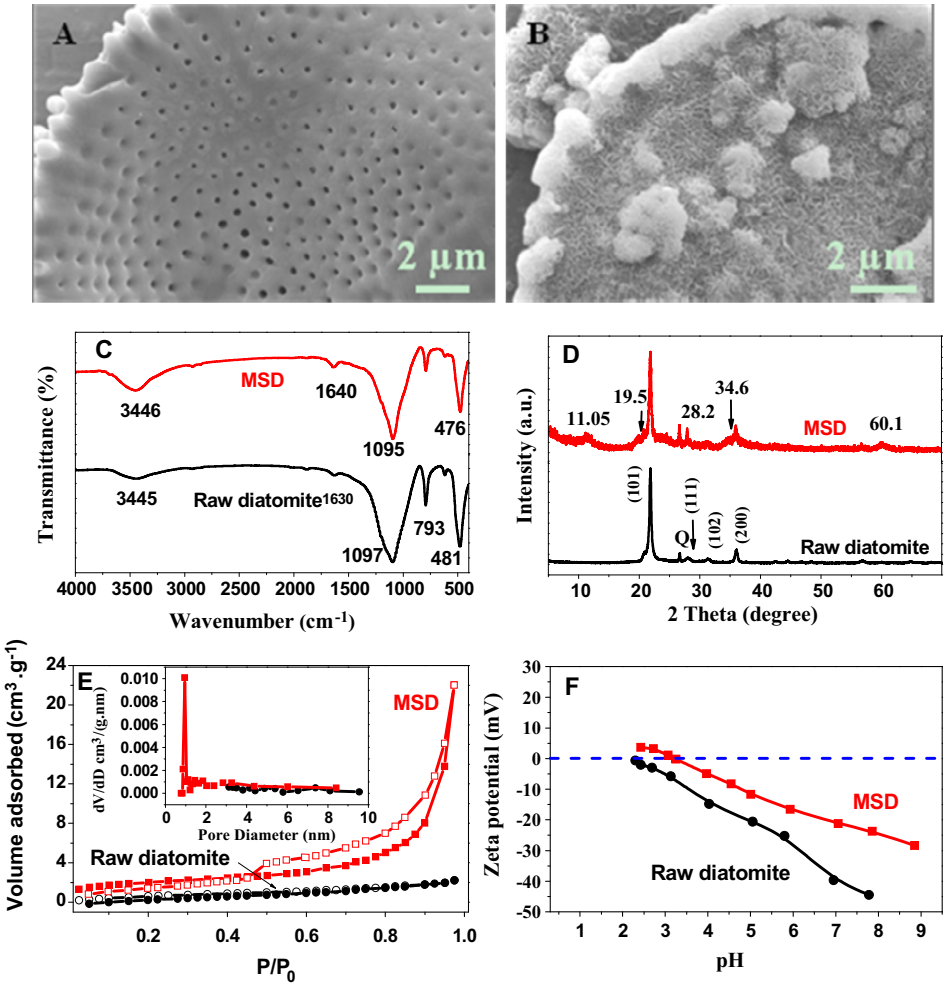

Fig. 1. Characterization of diatomite and MSD. (A and B) SEM images of raw diatomite and MSD, respectively; (C) FT-IR spectra; (D) XRD patterns; (E) N_2 adsorption-desorption isotherms, the inserted curves: the distribution of pore size; (F) zeta potentials, m/V = 0.5 g/L, I = 0.01 mol/L $NaNO_3$ and T = 293 K.

(1 0 1), (1 1 1), (1 0 2) and (2 0 0) planes of SiO_2 (JCPDS card no. 39-1425), respectively. For MSD, low intensity peaks at 2θ = 19.5, 34.6 and 60.1° were correspond to the (0 2 0), (2 0 0) and (3 3 2) planes of magnesium silicate (JCPDS card no. 03-0174). Besides, the two peaks at 2θ = 11.1 and 28.2° were also attributed to magnesium silicate phase (JCPDS card no. 03-0519). The other main characteristic peaks for MSD indicated the stability of the crystalline phase of diatomite during hydrothermal process. The results suggested that the poorly crystalline of magnesium silicate was hydrothermally synthesized on the surface of diatomite.

Based on the nitrogen isotherms shown in Fig. 1E, the specific surface area of diatomite and MSD calculated by the BET method were 1.170 and 12.068 m^2/g, respectively. The high BET surface area of MSD was mainly due to the abundant micropores exposed on the surface of diatomite. According to the calculation from BJH (Barrett-Joiner-Halenda) method, the total pore volume of diatomite and MSD are 0.003 and 0.037 cm^3/g, respectively. As inserted pore size distribution curves in Fig. 1E, the MSD presented an obvious feature of micropores, whereas the diatomite displayed mesopores and macriopores. As shown by zeta potential in Fig. 1F, the isoelectric point values of MSD and diatomite were 3.2 and 2.5, respectively. The enhanced isoelectric point value of MSD might be due to the surface generated magnesium silicate phase [21].

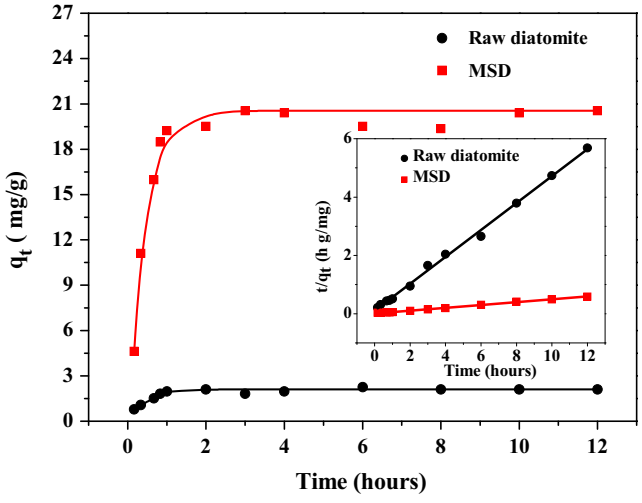

Fig. 2. Sorption kinetics of U(VI) on diatomite and MSD, inserted curve: the fitting of the pseudo-second order kinetic model, pH = 5.0, C_0 = 24 mg/L, m/V = 0.5 g/L, I = 0.01 mol/L $NaNO_3$, T = 293 K.

3.2. Sorption kinetics

Fig. 2 shows the sorption kinetics of U(VI) on MSD and diatomite at pH 5.0. It is observed that the amount and rate of U(VI) sorption on MSD were higher than that on diatomite. The sorption of U(VI) on diatomite and MSD rapidly increased at the first 3 h and then maintained the high level sorption after contact time more than 3 h. It is proposed that the fast removal rate was attributed to the more sorption active sites of MSD, which facilitated the diffusion of U(VI) from bulk solution onto the surface binding sites [4,30]. The results suggested that MSD can quickly eliminate radionuclides in potential practical application [31].

The pseudo-first and pseudo-second-order kinetic models were employed to simulate the data of sorption kinetics. The equations of the pseudo-first and pseudo- second-order kinetic models can be described as Eqs. (8) and (9), respectively [32,33].

$$\ln(q_e - q_t) = \ln q_e - k_1 \times t \quad (8)$$

$$\frac{t}{q_t} = \frac{1}{k_2 \times q_e^2} + \frac{t}{q_e} \quad (9)$$

where k_1 and k_2 (g/(mg h)) are the rate constants of pseudo-first and pseudo-second- order model, respectively. q_e and q_t (mg/g) are the sorbed amount of U(VI) at equilibrium and time t (h), respectively. The corresponding parameters were summarized in Table 1.

As shown inset of linear plot feature of t/q_t versus t in Fig. 2, the sorption of U(VI) on MSD and diatomite can be satisfactorily simulated by pseudo-second-order model with high correlation coefficient ($R^2 = 0.997$). As summarized in Table 1, the equilibrium sorption capacity of U(VI) on MSD was higher than that of U(VI) sorption on diatomite.

3.3. Effect of pH and ionic strength

The effect of pH and ionic strength on sorption of U(VI) on diatomite and MSD are given in Fig. 3. The sorption of U(VI) on MSD was much higher than that diatomite. Magnesium silicate produced on the diatomite surface enlarged the specific sorption sites. Besides, the magnesium silicate homogeneous dispersed on the surface of diatomite formed a uniform exposed structure, which can enhance the sorption capacity according to the report [34]. As shown in Fig. 3, the sorption of U(VI) on diatomite and MSD increased with increasing pH from 3.0 to 6.0, then remained the steady state at pH 6.0–7.5, whereas the decrease of U(VI) sorption was observed at pH > 7.5. As shown in Fig. S1 in Supplementary materials, the predominate species of U(VI) in aqueous solution was UO_2^{2+} at pH < 5.0, and more multiple positive charged U(VI) species (e. g, $UO_2(OH)^+$, $(UO_2)_3(OH)_5^+$, and $(UO_2)_4(OH)_7^+$ species) were observed at pH 5.0–8.0, whereas the negative charged U(VI) species (i.e., $UO_2(CO_3)_2^{2-}$, $UO_2(CO_3)_3^{4-}$ species) were observed at pH > 8.0. As shown in Fig. 1F, the surface of MSD and diatomite was negative at pH > 4.0. Consequently, the increased sorption of U(VI) on MSD and diatomite at pH 3.0–6.0 was due to the electrostatic attraction between positive charged U(VI) species and negative adsorbent surface, whereas the decreased sorption of U(VI) on MSD at pH > 7.0 was attributed to the electrostatic repulsion of negative adsorbent surface and negative charged U(VI) species such as $UO_2(CO_3)_2^{2-}$ and $UO_2(CO_3)_3^{4-}$ species [35].

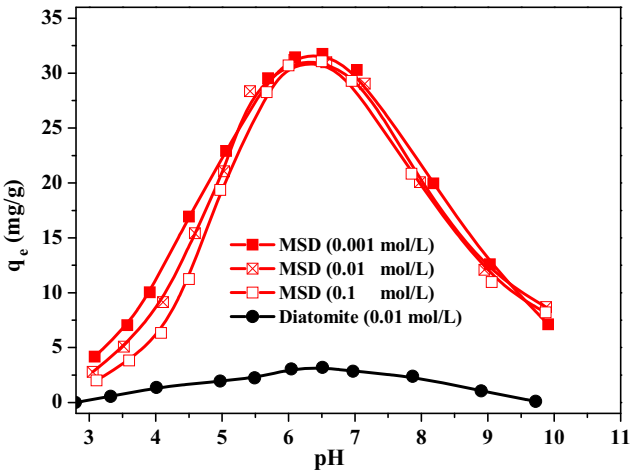

Fig. 3. Effect of pH on the sorption of U(VI) on diatomite and MSD, $C_0 = 24$ mg/L, $m/V = 0.5$ g/L and $T = 293$ K.

The effect of ionic strength on U(VI) sorption onto MSD was also illustrated in Fig. 3. The sorption of U(VI) on MSD decreased with increasing ionic strength at pH < 4.0, whereas the sorption of U (VI) on MSD was independent of ionic strength at pH > 5.0. It is reported that the outer-sphere surface complexation/cation exchange was sensitive to ionic strength, whereas inner-sphere surface complexation was independent of ionic strength [36–38]. Consequently, outer-sphere surface complexation/cation exchange dominated the sorption of U(VI) on MSD at the low pH, whereas inner-sphere surface complexation mechanism dominated the sorption of U(VI) on MSD at high pH values.

3.4. Sorption isotherms

Fig. 4A shows the sorption isotherms of U(VI) on MSD in the presence of 0.01 mol/L $NaNO_3$. The sorption of U(VI) on MSD increased with increasing temperature, indicating the interaction of U(VI) with MSD was promoted at higher temperature. The Langmuir and Freundlich models were used to simulate the sorption data. The Langmuir isotherm model usually described the monolayer sorption process that took place on a homogeneous surface. The Freundlich expression is an exponential equation that represents properly the sorption data at low and intermediate concentrations on heterogeneous surfaces [3]. The equations of Langmuir and Frenudlich models can be expressed as Eqs. (10) and (11), respectively [39,40]:

$$q_e = \frac{bq_{max}C_e}{1 + bC_e} \quad (10)$$

$$q_e = K_F C_e^n \quad (11)$$

where q_{max} (mg/g) is the amount of U(VI) at complete monolayer coverage; b (L/mg) is a constant that relates to the heat of sorption.

Table 1
Kinetic parameters of U(VI) sorption on raw diatomite and MSD.

System	Pseudo-first-order			Pseudo-second-order		
	q_e (mg/g)	K_1 (g/(mg h))	R^2	q_e (mg/g)	K_2 (g/(mg h))	R^2
Diatomite	8.808	0.0721	0.3656	2.17	1.93	0.997
MSD	23.4718	0.003	0.3956	20.72	0.22	0.997

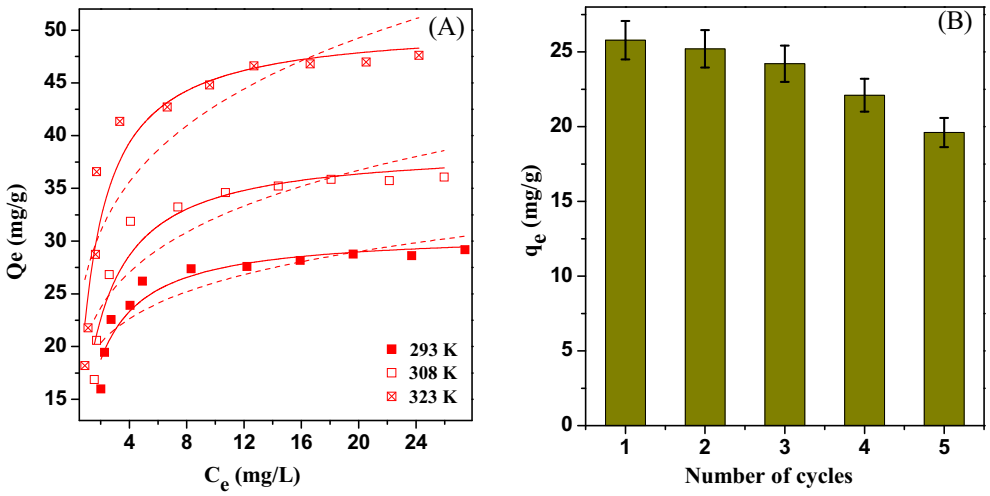

Fig. 4. (A) Sorption isotherms of U(VI) on MSD at three different temperatures, solid and dashed lines: Langmuir and Freundlich model, respectively. (B) Recycling of MSD for U(VI) removal using 0.5 mol/L Na_2CO_3 as a desorption agent, pH = 5.0, m/V = 0.5 g/L, I = 0.01 mol/L $NaNO_3$ and T = 293 K.

K_F ($mg^{(1-n)}L^n/g$) is the Freundlich constant and n represents the degree of sorption dependence at equilibrium concentration. The corresponding parameters of the Langmuir and Freundlich equations were listed in Table 2. As shown in Table 2, the sorption of U(VI) on MSD was better simulated by the Langmuir model than that of the Freundlich model. The q_{max} values of MSD and diatomite calculated from the Langmuir model at pH 5.0 and 273 K were 31.54 and 12.74 mg/g, respectively. As shown in Table 3, the sorption capacity of U(VI) on MSD was significantly higher than other adsorbents such as sepiolite [4], attapulgite [41], quercetin modified Fe_3O_4@SiO_2 [42], Na-montomorillonite [8], modified silica gel [43]. These findings indicated that MSD possessed obvious superiority in sorption capacity.

The thermodynamic parameters were calculated based on the sorption isotherms at the three different temperatures. The more details on the calculation of the standard free energy change-ΔG^0, standard enthalpy change-ΔH^0 and the standard entropy change-ΔS^0 were provided in Supporting Information (SI). As shown in Table 4, the negative ΔG^0 values (i.e., −5.10, −6.20 and −7.90 kJ/mol for U(VI) at 293, 308 and 323 K, respectively) indicated that U(VI) sorption on MSD was a spontaneous process.

Table 4
Thermodynamic parameters for U(VI) sorption on MSD.

T (K)	ΔG (kJ/mol)	ΔS (J/(mol K))	ΔH (kJ/mol)
293	−5.10		
308	−6.20	93.63	22.44
323	−7.90		

Concurrently, the decreased values of ΔG^0 with increasing temperature indicated that the sorption reaction was more favorable at the higher temperature. The positive value ΔH^0 (22.44 kJ/mol) suggested that U(VI) sorption on MSD was an endothermic process. The interaction between U(VI) and MSD combined with two process: the endothermic process of dehydration of U(VI) from aqueous solution and the exothermic process of attachment of U (VI) to MSD surface [4]. Therefore, it was inferred that the endothermicity of the dehydration process exceeded the exothermicity of attachment of U(VI) to MSD surface. The positive ΔS^0 value (93.63 J/mol/K) implied some structural changes in U(VI) on MSD during the sorption process, which leads to an increase in the disorder of the solid–solution system. The thermodynamic

Table 2
Parameters of Langmuir and Freundlich models for U(VI) sorption on MSD.

T (K)	Langmuir model			Freundlich model		
	q_{max} (mg/g)	b (L/mg)	R^2	k_F ($mg^{(1-n)}$ L^n/g)	n	R^2
293	31.54	0.62	0.86	16.54	0.19	0.71
308	39.28	0.66	0.89	19.39	0.22	0.75
323	50.33	0.91	0.94	25.69	0.22	0.82

Table 3
Comparison of U(VI) sorption capacity of MSD with other sorbents.

Sorbents	Exp. conditions		q_{max} (mg/g)	Reference
	pH	T (K)		
Sepiolite	6.0	313	18.47	[4]
Attapulgite	4.0	303	12.98	[33]
Fe_3O_4@SiO_2	3.7	298	12.33	[34]
Na-montomorillonite	4.9	298	9.15	[7]
Modified silica gel	6.0	298	8.46	[35]
MSD	5.0	293	31.54	This work

parameters indicated that the sorption of U(VI) on MSD was an endothermic and spontaneous process.

3.5. Regeneration and reusability

From the viewpoints of low economic cost and environmental renewable, it is important to recycle these adsorbents in environmental cleanup. Therefore, the recycling of MSD in the sorption of U(VI) was investigated as followed: After sorption equilibrium, the adsorbent was dispersed in 20 mL of 0.5 M Na_2CO_3 solution for 24 h, and then the suspension was centrifuged and the sorbent was washed with Milli-Q water, and then MSD was dried at 60 °C. As shown in Fig. 4B, the sorption of U(VI) on MSD slightly decreased after 5 cycles, indicating that MSD has a good reusability. The inappreciable reduction in sorption capacity was charged upon the incomplete desorption of U(VI) from MSD composite by strong covalent bond.

3.6. XPS analysis

The sorption mechanism of U(VI) on MSD was demonstrated by XPS technology. Fig. 5 shows the normalized survey and high resolution scans (O 1s, Si 2p and U4f) of XPS spectra of MSD and MSD-U(VI) samples. After the U(VI) sorption, the clear peak of U 4f indicated that U(VI) was immobilized on the surface of MSD. As shown in Fig. 5B, the O 1s spectrum of MSD showed three peaks at 531.0,

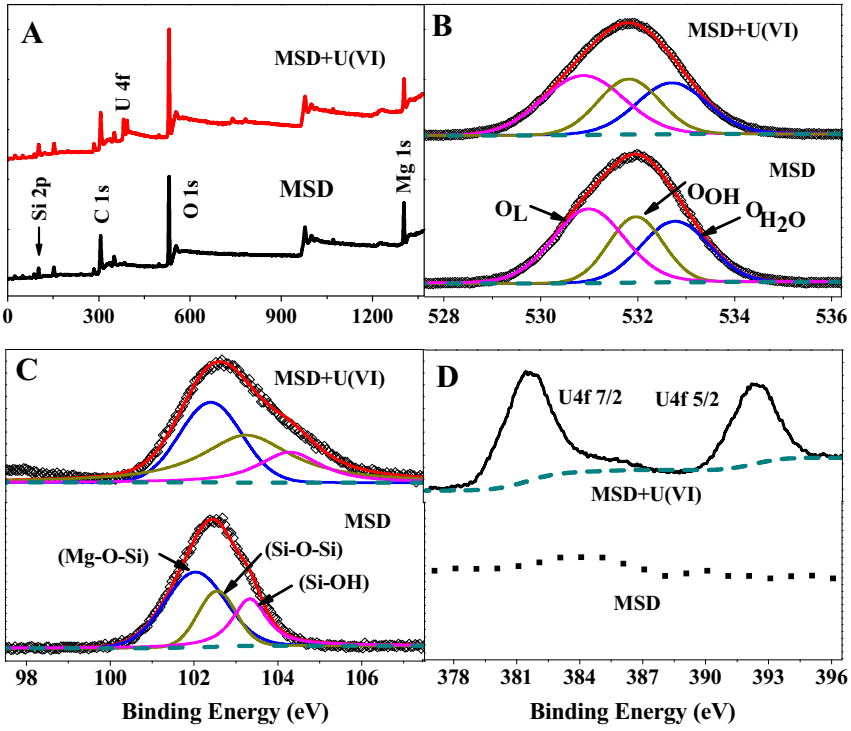

Fig. 5. XPS analysis of MSD before and after U(VI) sorption, (A) total survey; (B and D) high resolutions of O 1s, Si 2p and U 4f, respectively.

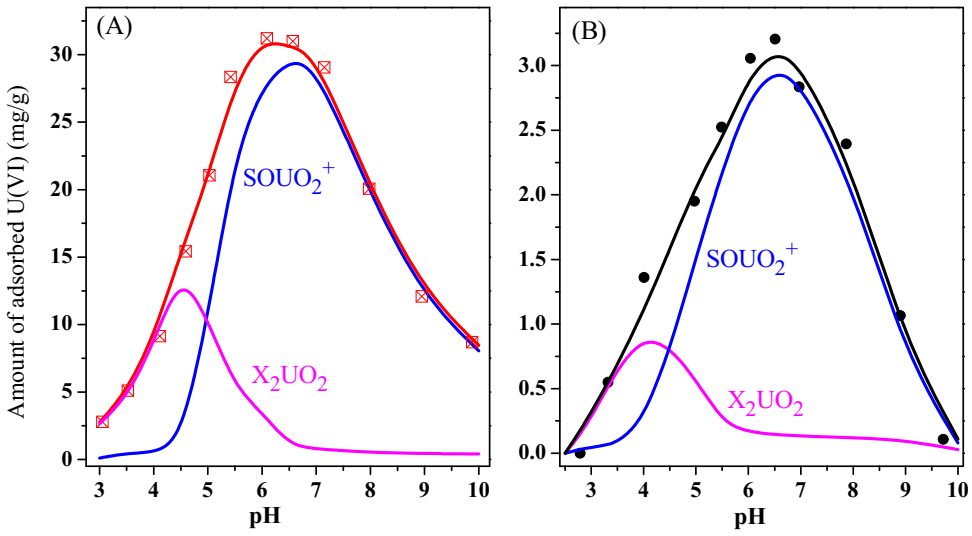

Fig. 6. Surface complexation modeling of U(VI) sorption on diatomite and MSD, C_0 = 24 mg/L, m/V = 0.5 g/L, I = 0.01 mol/L $NaNO_3$ and T = 293 K.

532.0 and 532.8 eV, which were corresponded to the surface lattice oxygen species (O_L), surface adsorbed hydroxyl species (O_{OH}) and adsorbed water molecules (O_{H2O}) on the diatomite surface in sequence, respectively [44,45]. According to Fig. 5C, three peaks Si 2p spectrum of MSD at ~102.1, 102.6 and 103.3 eV were in agreement with the literature reporting data for the binding energy (BE) value of the Si 2p from the Mg—O—Si, Si—O—Si and Si—OH, respectively [46,47]. As shown in Fig. 5B and C, O 1s spectrum after sorption shifted to lower binding energy, while Si 2p spectrum shifted to higher binding energy. For example, the binding energies of O_L and O_{OH} were shifted from 531.0 to 530.8 eV and from 532.0 to 531.8 eV, respectively, whereas the binding energies of Mg—O—Si, Si—O—Si and Si—OH groups were shifted from 102.1 to 102.4 eV, from 102.6 to 103.3 eV and from 103.3 to 104.3 eV, respectively. As shown in Fig. 5D, U 4f spectrum displayed two splitting peaks such as at around 382.0 and 392.0 eV for U $4f_{7/2}$ and U $4f_{5/2}$, respectively [48]. The XPS results indicated that oxygen-containing functional groups were responsible to the high effective sorption of U(VI) on MSD.

3.7. Surface complexation modeling

Fig. 6A and B shows the surface complexation modeling of U(VI) sorption on MSD and diatomite, respectively. One can see that the sorption of U(VI) on MSD and diatomite can be satisfactorily fitted by diffuse layer model with cation exchange (X_2UO_2 species) and inner-sphere surface complexation ($SOUO_2^+$ species). As shown in Fig. 6A and B, the main adsorbed U(VI) species were X_2UO_2 species at pH < 4.0, whereas $SOUO_2^+$ species dominated the U(VI) sorption at pH > 5.0. The fitted results of surface complexation modeling indicated that the sorption of U(VI) on MSD and diatomite at pH < 4.0 was cation exchange, whereas inner-sphere surface complexation dominated the sorption of U(VI0 on MSD and diatomite at pH > 5.0.

4. Conclusions

The novel MSD sorbent was prepared successfully using a facile hydrothermal method, which provided an environment-friendly and cost-effective method to design a green, efficient sorption material. The maximum sorption capacity of U(VI) on MSD at pH 5.0 and 293 K was 31.54 mg/g, which was significantly higher than of natural clay minerals. According to the analysis of XPS spectra, the oxygen containing functional groups (e.g., Si—OH) were responsible for the sorption of U(VI) on MSD. The results of surface complexation modeling indicated that cation exchange and inner-sphere surface complexation dominated the sorption of U(VI) on MSD and diatomite at pH < 4.0 and pH > 5.0, respectively. These findings revealed that MSD can be used a promising sorbent for pre-concentration and immobilization of radionuclides in nuclear waste management.

Acknowledgments

Financial supports from National Natural Science Foundation of China (21377132, 41273134, 21307135, 91326202), and Chinese National Fusion Project for ITER (No. 2013GB110004) are acknowledged.

Appendix A. Supplementary material

Supplementary data associated with this article can be found, in the online version, at http://dx.doi.org/10.1016/j.seppur.2016.09.052.

References

[1] R. Zhang, C.L. Chen, J. Li, X.K. Wang, J. Colloid Interface Sci. 460 (2015) 237–246.
[2] G.X. Zhao, T. Wen, X. Yang, S.B. Yang, J.L. Liao, J. Hu, D.D. Shao, X.K. Wang, Dalton Trans. 41 (2012) 6182–6188.
[3] C.C. Ding, W.C. Cheng, Y.B. Sun, X.K. Wang, J. Hazard. Mater. 295 (2015) 127–137.
[4] Y.B. Sun, J.X. Li, X.K. Wang, Geochim. Cosmochim. Acta 140 (2014) 621–643.
[5] A.P. Kryvoruchko, L. Yu, I.D. Atamanenko, B.Y. Kornilovich, Desalination 162 (2004) 229–236.
[6] B.H. Gu, Y.K. Ku, P.M. Jardine, Environ. Sci. Technol. 38 (2004) 3184–3188.
[7] M. Irani, M. Amjadi, M.A. Mousavian, Chem. Eng. J. 178 (2011) 317–323.
[8] R. Zhang, C.L. Chen, J. Li, X.K. Wang, Appl. Surf. Sci. 349 (2015) 129–137.
[9] M.A.M. Khraisheh, Y.S. Al-Degs, W.A.M. McMinn, Chem. Eng. J. 99 (2004) 177–184.
[10] G.D. Sheng, S.T. Yang, J. Sheng, J. Hu, X.L. Tan, X.K. Wang, Environ. Sci. Technol. 45 (2011) 7718–7726.
[11] X.X. Ye, S.H. Kang, H.M. Wang, H.Y. Li, Y.X. Zhang, G.Z. Wang, H.J. Zhao, J. Hazard. Mater. 289 (2015) 210–218.
[12] W.B. Yu, P. Yuan, D. Liu, L.L. Deng, W.W. Yuan, B. Tao, H.F. Cheng, F.R. Chen, J. Hazard. Mater. 285 (2015) 173–181.
[13] Y.C. Du, H.G. Fan, L.P. Wang, J.S. Wang, J.S. Wu, H.X. Dai, J. Mater. Chem. A 1 (2013) 7729–7737.
[14] Y.C. Du, L.P. Wang, J.S. Wang, G.W. Zheng, J.S. Wu, H.X. Dai, J. Environ. Sci. 29 (2015) 71–81.
[15] Y.C. Du, G.W. Zheng, J.S. Wang, L.P. Wang, J.S. Wu, H.X. Dai, Micropor. Mesopor. Mater. 200 (2014) 27–34.
[16] W.B. Yu, L.L. Deng, P. Yuan, D. Liu, W.W. Yuan, P. Liu, H.P. He, Z.H. Li, F.R. Chen, J. Colloid Interface Sci. 448 (2015) 545–552.
[17] L.C. Zheng, C.G. Wang, Y.H. Shu, X.M. Yan, L.S. Li, Colloid Surf. A 468 (2015) 129–139.
[18] M. Kara, H. Yuzer, E. Sabah, M.S. Celik, Water Res. 37 (2003) 224–232.
[19] Q.Q. Ou, L. Zhou, S.G. Zhao, H.J. Geng, J.J. Hao, Y.Y. Xu, H.L. Chen, X.G. Chen, Chem. Eng. J. 180 (2012) 121–127.
[20] A. Rodriguez, G. Ovejero, M. Mestanza, J. Garcia, Ind. Eng. Chem. Res. 49 (2010) 3207–3216.
[21] Y.Q. Wang, G.Z. Wang, H.Q. Wang, C.H. Liang, W.P. Cai, L.D. Zhang, Chem. Eur. J. 16 (2010) 3497–3503.
[22] S.W. Zhang, W.Q. Xu, M.Y. Zeng, J. Li, J.X. Li, J.Z. Xu, X.K. Wang, J. Mater. Chem. A 1 (2013) 11691–11697.
[23] H.P. van Leeuwen, John Wiley and Sons, Chichester, 2000.
[24] R.O. James, G.A. Parks, Plenum Press, New York, 1982, vol. 12, pp. 119–216.
[25] Y.B. Sun, Z.-Y. Wu, X.X. Wang, C.C. Ding, W.C. Cheng, S.-H. Yu, X.K. Wang, Environ. Sci. Technol. 50 (2016) 4459–4467.
[26] C.C. Ding, W.C. Cheng, X.X. Wang, Z.-Y. Wu, Y.B. Sun, C.L. Chen, X.K. Wang, S.-H. Yu, J. Hazard. Mater. 313 (2016) 253–261.
[27] S.K. Padmanabhan, S. Pal, E.U. Haq, A. Licciulli, Appl. Catal. B 485 (2014) 157–162.
[28] S. Yusan, A. Bampaiti, S. Aytas, S. Erenturk, M.A.A. Aslani, Ceram. Int. 42 (2016) 2158–2163.
[29] Y.B. Sun, R. Zhang, C.C. Ding, X.X. Wang, W.C. Cheng, C.L. Chen, X.K. Wang, Geochim. Cosmochim. Acta 180 (2016) 51–65.
[30] P. Yuan, D.Q. Wu, H.P. He, Z.Y. Lin, Appl. Surf. Sci. 227 (2004) 30–39.
[31] Y.B. Sun, C.L. Chen, D.D. Shao, J.X. Li, X.L. Tan, G.X. Zhao, S.B. Yang, X.K. Wang, RSC Adv. 2 (2012) 10359–10364.
[32] J. Li, S.W. Zhang, C.L. Chen, G.X. Zhao, X. Yang, J.X. Li, X.K. Wang, ACS Appl. Mater. Interface 4 (2012) 4991–5000.
[33] T. Wen, X.L. Wu, X.L. Tan, X.K. Wang, A.W. Xu, ACS Appl. Mater. Interface 5 (2013) 3304–3311.
[34] C.X. Gui, Q.Q. Wang, S.M. Hao, J. Qu, P.P. Huang, C.Y. Cao, W.G. Song, Z.Z. Yu, ACS Appl. Mater. Interface 6 (2014) 14653–14659.
[35] Y.B. Sun, S.B. Yang, Y. Chen, C.C. Ding, W.C. Cheng, X.K. Wang, Environ. Sci. Technol. 49 (2015) 4255–4262.
[36] M.H. Bradbury, B. Baeyens, Geochim. Cosmochim. Acta 66 (2002) 2325–2334.
[37] Y.B. Sun, D.D. Shao, C.L. Chen, S.B. Yang, X.K. Wang, Environ. Sci. Technol. 47 (2013) 9904–9910.
[38] Y.B. Sun, Q. Wang, C.L. Chen, X.L. Tan, X.K. Wang, Environ. Sci. Technol. 46 (2012) 6020–6027.
[39] X.L. Tan, X.K. Wang, M. Fang, C.L. Chen, Colloid Surf. A 296 (2007) 109–116.
[40] X.L. Tan, C.L. Chen, S.M. Yu, X.K. Wang, Appl. Geochem. 23 (2008) 2767–2777.
[41] W.C. Cheng, C.C. Ding, Y.B. Sun, X.K. Wang, Chem. Eng. J. 269 (2015) 1–8.
[42] S. Sadeghi, H. Azhdari, H. Arabi, A.Z. Moghaddam, J. Hazard. Mater. 215 (2012) 208–216.
[43] G.K. Incili, G.A. Aycik, J. Radioanal. Nucl. Chem. 302 (2014) 79–85.
[44] L.Y. Jiang, L. Liu, S.D. Xiao, J.M. Chen, Chem. Eng. J. 284 (2016) 609–619.
[45] D.N. Li, X.J. Ma, X.Y. Liu, L.L. Yu, Bioresources 9 (2014) 602–612.
[46] R. Brambilla, C. Radtke, J.H.Z. Dos Santos, M.S.L. Miranda, J. Sol-Gel Sci. Technol. 51 (2009) 70–77.
[47] S.C. Ma, Z.G. Wang, J.L. Zhang, D.H. Sun, G.X. Liu, Appl. Surf. Sci. 327 (2015) 453–461.
[48] C.C. Ding, W.C. Cheng, Y.B. Sun, X.K. Wang, Geochim. Cosmochim. Acta 165 (2015) 86–107.